J. Fluid Mech. (2014), *vol.* 749, *pp.* 649–665. © Cambridge University Press 2014
doi:10.1017/jfm.2014.220

Vortices, dissipation and flow transition in volatile binary drops

R. Bennacer[1] **and K. Sefiane**[2,†]

[1]LMT, Ecole Normale Superieure Cachan, F-94235 Cachan, France

[2]School of Engineering, The University of Edinburgh, Edinburgh EH9 3JL, UK

(Received 29 October 2013; revised 31 March 2014; accepted 15 April 2014;
first published online 22 May 2014)

Despite its fundamental and practical relevance, flow structure and evolution within volatile mixture drops remains largely unexplored. We study experimentally, using particle image velocimetry (PIV), the evolution of internal flow during the evaporation of ethanol–water mixture drops for different initial concentrations. The investigation revealed the existence of three stages in the evolving flow behaviour within these binary volatile drops. We propose an analysis of the nature of the flow and focus on understanding successive flow stages as well as transition from multiple vortices to a monotonic outward flow. We show that the existence of multiple vortices during the first stage is driven by local concentration gradients along the interface. When the more volatile component (in this case ethanol) is depleted, the intensity of this Marangoni flow abruptly declines. Towards the end of the first stage, ethanol is driven from the bulk of the drop to the interface to sustain weakening concentration gradients. Once these gradients are too weak, the solutal Marangoni number becomes sub-critical and the driving force for the flow switches off. The evolution of flow structure and transition between stages is found to be well correlated with the ratio of Marangoni and Reynolds numbers. Furthermore, we argue that whilst the observed vortices are driven by surface tension shear stress originating at the liquid/vapour interface, the transition in flow and its dynamics is entirely determined by viscous dissipation. The comparison between the analytical expression for vorticity decay based on viscous dissipation and the experimental data shows a very good agreement. The analysis also shows that regardless of the initial concentration, for same sized drops, the transition in flow follows exactly the same trend. This further supports the hypothesis of a viscous dissipation transition of the flow. The last stage is satisfactorily explained based on non-uniform evaporation and continuity-driven flow.

Key words: Marangoni flows, drops

1. Introduction

Since the pioneering work of Young (1805), the interaction of liquid drops with solid substrates has been a subject of interest to scientists for more than two centuries. This phenomenon, known as wetting, is recognised as being crucial in a wide range of biological, natural and industrial processes. When drops are deposited on solids

† Email address for correspondence: ksefiane@ed.ac.uk

https://doi.org/10.1017/jfm.2014.220 Published online by Cambridge University Press

in an unsaturated atmosphere, they evaporate at a rate which depends on relative saturation and ambient conditions. This process of evaporation and drying of sessile drops on solid substrates has attracted wide interest amongst researchers over the last decade (Deegan *et al.* 1997; Hu & Larson 2006; Sefiane *et al.* 2009; Erbil 2012). The evaporation of drops and their profile evolution and dependence on ambient conditions has been the subject of numerous studies. Various aspects of this phenomenon have been experimentally and theoretically explored, including diffusion of vapour in the ambient medium (Sefiane *et al.* 2009) and substrate properties (Sefiane & Bennacer 2011). The dynamics of the drop profile and three-phase contact line and their dependence on substrate roughness and properties has also been extensively researched. A recent review on this topic with a more detailed description of the phenomenon can be found in Erbil (2012).

Besides the evolution of drop profiles and the kinetics of evaporation another aspect, equally important, that has attracted the attention of researchers is the characteristics, nature and evolution of the flow within these volatile drops. In small enough evaporating drops, fluid flow can be driven either by continuity (Deegan *et al.* 1997), or surface tension gradients (Hu & Larson 2006), i.e. the Marangoni effect. In the case of single-component drops, the continuity flow is found to be mainly an outward flow driven by mass conservation (Deegan *et al.* 1997; Hamamoto, Christy & Sefiane 2011). Another widely accepted origin of the flow in volatile drops is lMarangoni flow driven by surface tension gradients (Hu & Larson 2006). The orientation and intensity of this flow in the case of single-component drops can depend on the relative thermal properties of the substrate and liquid (Ristenpart *et al.* 2007). Furthermore, these flows can be the result of temperature and/or concentration gradients and may play a major role in energy transport (Ghasemi & Ward 2010). Generally, surface-tension-driven flows in single-component volatile drops are essentially thermocapillary in nature, i.e. driven by temperature gradients.

In comparison with single-component evaporating drops, the evaporation of binary and multicomponent drops in general has received rather limited attention (Rowan *et al.* 2000; Sefiane, David & Shanahan 2008). The few existing studies have focused essentially on studying the evolution of the profile of the mixture drop. Researchers agree on the observation that evaporation proceeds in distinct stages, a first stage where the more volatile component evaporates, a second stage which is a mixed stage and a last stage where the drop behaves as if it mainly consists of the less volatile component. These evaporation stages have been revealed through observations and measurements of the drop profile such as the angle, height, volume and base (Cheng, Soolaman & Yu 2006; Hopkins & Reid 2006). It is worth stressing that during the evaporation of binary mixture drops, additional physical mechanisms, which are absent in single-component drops contribute to the observed behaviour. Because of selective evaporation, the more volatile component evaporates first. This component has to diffuse from the bulk liquid of the drop to the interface. Once at the interface it evaporates and then diffuses in the gas phase, usually a mixture of vapour and air. This process continues until the more volatile component is depleted and the remaining volume is essentially comprised of the less volatile one. Some traces of the volatile component could however persist till the end of the drop lifetime.

As far as surface tension flows are concerned, the evaporation of binary mixture drops introduces a new effect which is not present in the case of single-component drops. This effect is related to local concentration gradients on the interface and the resulting surface tension stresses and solutal Marangoni flows. Recently, a study used particle image velocimetry (PIV) to characterise the flow within an evaporating binary

https://doi.org/10.1017/jfm.2014.220 Published online by Cambridge University Press

mixture drop consisting of ethanol and water (Christy, Hamamoto & Sefiane 2011). This study revealed the existence of three stages in flow structure. The first stage corresponds to the existence of multiple convection vortices, the number of which reduces in time until the end of the first stage. The second stage, the transition stage, corresponds to a transition of the flow structure from multiple vortices to an outward flow (the third stage) which is typical of pure water evaporating drops. The transition occurs very rapidly, in few seconds and the evolution of vorticity intensity in time exhibits an exponential decay. In an attempt to explain these observations it has been suggested that diffusion of the final part of ethanol in the liquid phase from the bulk to the interface could be the physical mechanism responsible for the transition in flow. Limited data however did not allow further exploration and quantification of the true mechanism(s) behind the observed transition in flow. It has been deduced, from Christy *et al.* (2011), that the observed flow structure in the first stage is driven by surface tension gradients on the interface. These surface tension gradients are a direct result of concentration gradients: the concentration of ethanol (or water) on the interface affects the surface tension locally. The local concentration of ethanol on the interface is a result of the various processes taking place, namely diffusion in liquid from the bulk to the interface, evaporation, and diffusion into the gas phase. Since there is a limited reservoir of ethanol within the drop, concentration gradients on the interface tend to evolve till evaporation is complete. The study of Christy *et al.* (2011) was however limited to one initial concentration namely 5 % of aqueous ethanol. Also the interpretation of the successive stages was not thoroughly examined.

It is clear that understanding of the nature of internal flow within evaporating drops in general is far from complete. Furthermore, the flow within binary volatile drops remains, to the best of our knowledge, largely unexplored. Amongst the outstanding questions is the role played by the initial concentration in the observed stages of flow. There is also no physical interpretation for each of the observed stages of evaporating binary drops. This paper presents new data on internal flow structure and transition during the evaporation of binary mixture drops. Ethanol–water drops at various initial concentrations, evaporating under ambient conditions are investigated using the PIV technique to reveal the flow field and its evolution. The study shows that a first stage in the evaporation process is characterised by multiple vortices whose number decreases in time. The space-averaged intensity of vorticity remains however fairly constant during this first stage. The transition from multiple vortices to an outward monotonic flow occurs during a relatively rapid stage characterised by an exponential decline in vorticity. When normalised with the initial vorticity of the first stage, the transition stage is found to follow the same trend for all initial concentrations whose decay constant depends on drop size.

The paper is organised as follows, in § 2 we present the experimental data on evaporation stages obtained from drop shape analysis and flow fields obtained using PIV for three initial concentrations, and discuss observed trends. In § 3 we perform an analysis of the main physical mechanisms likely to be responsible for the observed flow. The first stage of evaporation is discussed in § 3.1. In § 3.2, we analyse the transition in flow and compare the analytical solution obtained from a model of viscous dissipation and decay of vorticity with the experimental data. Finally in § 3.3, we discuss the outward flow observed in the last stage of evaporation.

2. Experimental results

The experimental setup and procedures are similar to those in Christy *et al.* (2011) and are briefly recalled hereafter. Ethanol–water mixture drops of 0.12 μl (±0.03 μl)

https://doi.org/10.1017/jfm.2014.220 Published online by Cambridge University Press

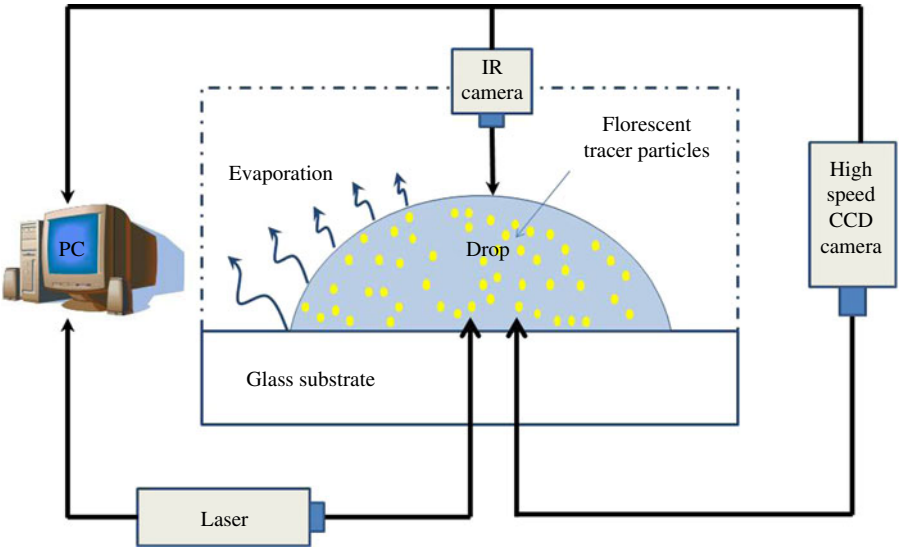


FIGURE 1. (Colour online) Schematic of the experimental setup.

volume are seeded with 0.04 % tracers of fluorescent micro-spheres (1 μm diameter, Nilered, carboxylate modified FluoSphere® beads of density 1.05 g cm^{-3}). The drops were deposited on a transparent glass substrate, sitting on an inverted microscope (Leica DM15000 M). The base radii of the sessile drops ranged from 0.9 to 1.1 mm, depending on ethanol concentration (0.9 mm for 5 %, 1 mm for 25 % and 1.1 mm for 50 %). A New Wave Pegasus pulse diode laser emitting at 527 nm illuminated the drops from beneath causing the particles to fluoresce at 575 nm. A high-speed Dantec Dynamics Nanosense II camera (512 × 512 pixels) is synchronized with the laser and captured the experiment at 20 or 100 Hz with a spatial resolution of 320 pixelspermm.

The PIV technique is used to map the flow in these ethanol–water mixture drops evaporating at ambient conditions. Imaging the drop from beneath revealed flow maps as cross-sections adjacent to the base of the drop, figures 1 and 4. The measured vorticity is a two-dimensional section and represents the intensity and structure of the flow in the drop. Profiles of flow velocity along the base radius of the drop are extracted and plotted versus time. Three initial ethanol in water concentrations were studied, 5 %, 25 % and 50 %, per volume. For the two higher concentrations a higher data acquisition frequency of 100 Hz is used instead of the 20 Hz used in the case of 5 %. The reason for this is the shorter lifetime and higher flow velocity for higher ethanol concentrations. Typical measured flow velocities during the first stage are 10^{-6} m s^{-1}, 10^{-5} m s^{-1} and 10^{-4} m s^{-1} for 5 %, 25 % and 50 % respectively.

2.1. *Evaporation stages*

In addition to PIV flow measurements, a drop shape analysis instrument DSA100 from Kruss GmbH was simultaneously used to measure volume and base diameter evolution in time. The evaporation rate as a function of time is thus deduced and plotted in figure 2. The data for evaporation rate indicate that during the first stage, stage I, the evaporation rate decreases for all concentrations studied. This is in contrast with the evaporation of a pure, pinned water drop, where evaporation rate remains fairly constant. The decrease in evaporation rate can be understood in terms

https://doi.org/10.1017/jfm.2014.220 Published online by Cambridge University Press

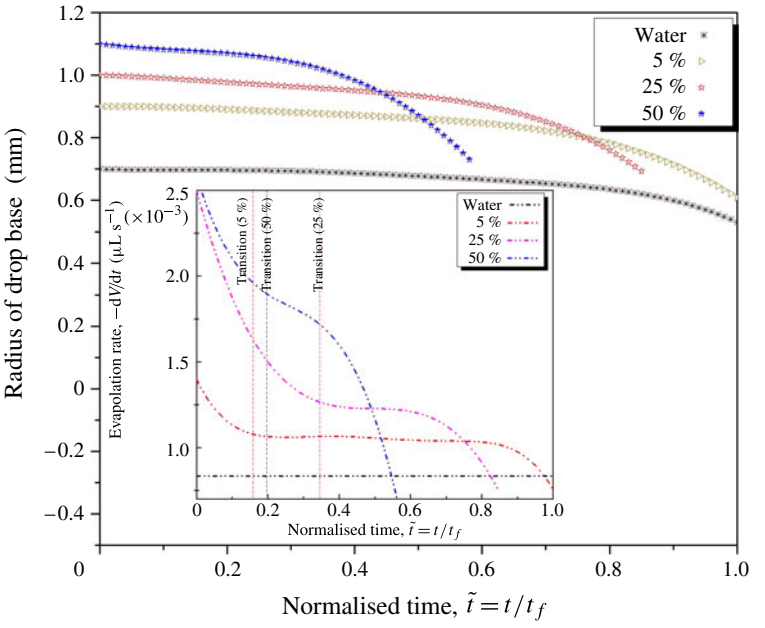


FIGURE 2. Drop radius evolution and evaporation rate (inset) in time for the three studied compositions and pure water for reference. The transition from stage I to stage II is highlighted. The transition, i.e. stage II, being very rapid, the first and last stages are the most noticeable.

of reduction of ethanol content. As shown by the vapour pressure equilibrium phase diagram, in figure 3 (inset), as ethanol concentration decreases, the vapour pressure decreases, hence so does evaporation. At the end of this decrease in evaporation rate, transition in flow structure occurs. The transition (stage II) is rapid and is followed by a constant evaporation rate similar to pure water during most of the last stage, stage III. The evaporation rate for a pure water drop is given in figure 2 as a reference. Evaporation rates tend to consistently increase with increasing ethanol initial concentration. On the other hand the lifetime of the drops decreases with increasing ethanol concentration.

The data for the base radius show that overall, the contact line remains pinned and sharply decreases towards the end of the drop lifetime, figure 2. This is due to the presence of tracer particles which tend to self-pin the contact line. The last stage in evaporation of mixture drops exhibits a plateau in the overall evaporation rate which is greater than the pure water case; this is probably due to the differences in drop base radii and to possible traces of ethanol left within the drop. It is worth noting that the transition in stage II occurs over a very short time, less than few seconds. It is also worth noting that the surface tension of a mixture, as expected, tends to change with concentration. The decrease in surface tension with increasing ethanol concentration is however not linear. The gradients in surface tension induced by concentration variations can be readily traced following the trend in figure 3.

2.2. *Flow structure evolution*

In order to represent the flow intensity across the base section of the drop, figure 4, a space-averaged vorticity is adopted; it is hereafter referred to as average vorticity,

https://doi.org/10.1017/jfm.2014.220 Published online by Cambridge University Press

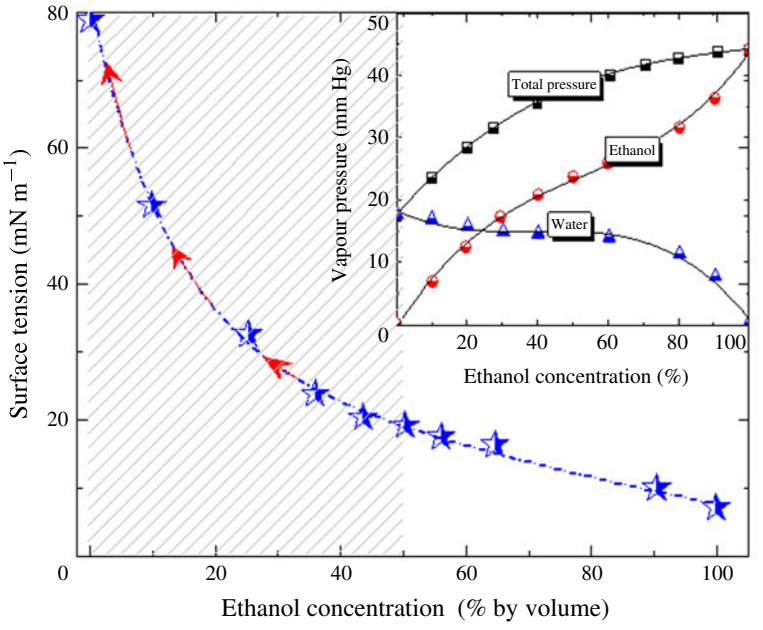


FIGURE 3. Surface tension of the binary mixture, the range of concentrations is hatched. Inset shows partial vapour pressure for water–ethanol mixture.

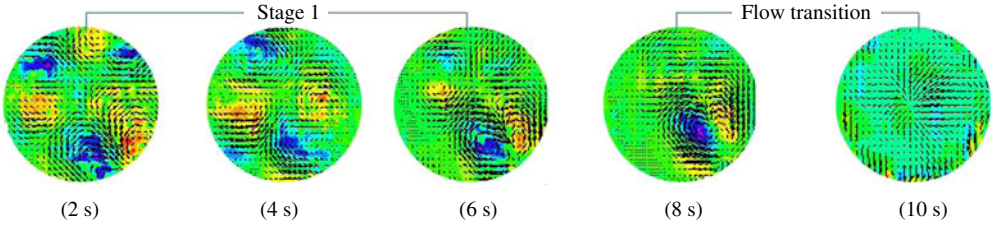


FIGURE 4. Flow structure evolution throughout the three distinct stages of evaporation for 50 % initial concentration. Velocity vectors and vorticity are superimposed, clockwise vorticity is represented in blue and counter-clockwise in red.

$\bar{\omega}_z(t)$. The results for spatio-temporal velocity, figure 5, as well as average vorticity, figure 6, show consistently, and for the three studied concentrations, three distinct stages in flow structure. During the first stage, multiple vortices are observed, their number reducing as evaporation proceeds. The intensity of average vorticity is found to be roughly constant during this stage albeit with some fluctuations. The onset of the first stage can be clearly seen as a sharp increase in average vorticity after the drop is deposited. This is more noticeable in the case of 25 % and 50 % concentrations though, figure 6. This first stage of constant average vorticity is followed by a decay in average vorticity intensity and finally an outward flow where vorticity is virtually nil which is reminiscent of evaporating pure water drops. The transition stage is characterised by a decay in average vorticity but also by a spike in radial velocity before settling into the last outward flow stage, figures 5 and 6. We can only speculate about the spike in velocity during transition; it is believed however that gradients along the interface intensify during the stage where the last traces of

https://doi.org/10.1017/jfm.2014.220 Published online by Cambridge University Press

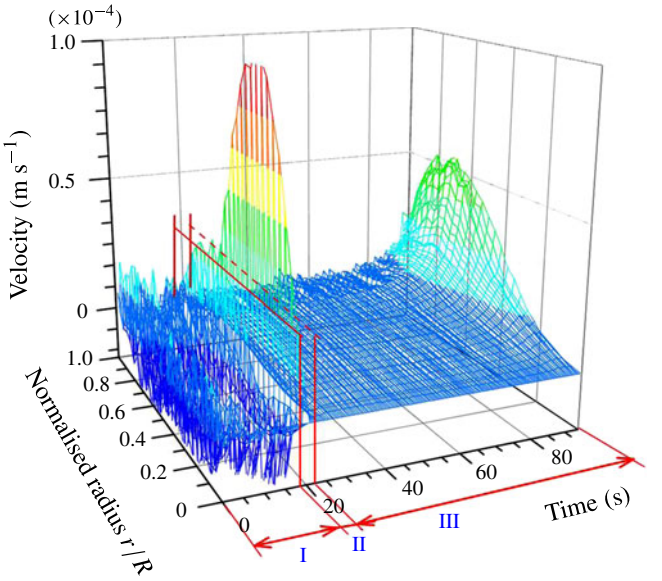


FIGURE 5. A sample of spatio-temporal evolution of the measured radial velocity for a 5 % ethanol binary evaporating drop. The three stages are highlighted, I multiple vortices, II transition and III outward flow.

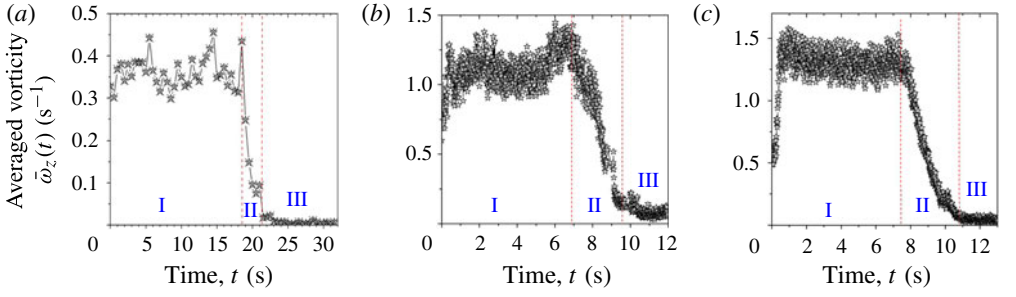


FIGURE 6. Evolution of averaged vorticity, $\bar{\omega}_z(t)$, in time for binary evaporating drops at initial ethanol concentrations of (*a*) 5 %, (*b*) 25 % and (*c*) 50 % by volume. Stages of evaporation are indicated.

ethanol evaporate from the surface. This might be due to some areas of the surface being significantly depleted in ethanol.

The intensity of the average vorticity, $\bar{\omega}_z(t)$, during the first stage is found to depend on the initial concentration. The lifetime of the drop as well as the extent of the successive stages are also dependent on the initial concentration. We can however, for the purpose of the analysis to follow, overcome this variability by normalising the average vorticity by the initial value, $\widetilde{\omega} = \langle\omega\rangle/\langle\omega_0\rangle$, and initialising the time by the transition time, $t^* = t - t_0$, as will be presented below. In so doing, one can compare the trends for various initial concentrations.

3. Analysis

In the following sections, the successive stages of evaporation and flow structure evolution within evaporating binary drops as revealed by the experimental data

https://doi.org/10.1017/jfm.2014.220 Published online by Cambridge University Press

presented above are analysed. Each stage is discussed with a focus on the physical mechanisms as well as interpretation of the observations.

3.1. *First stage of evaporation, multiple vortices*

In order to understand the nature of the observed flow we proceed by considering potential physical mechanisms responsible for the observed flow. Convection in a system such as the one under investigation, i.e. volatile small drops, can be either gravity or surface-tension (Marangoni) driven. The conditions for the onset of buoyancy, thermal or solutal Marangoni convection are determined by relevant dimensionless numbers. These are Rayleigh number, $Ra = (\Delta C(\partial\gamma/\partial C)L^3 g)/(D\nu)$ and thermal or solutal Marangoni number, $Ma_s = ((\partial\gamma/\partial C)\Delta CL)/(\mu D_l)$, respectively. γ being liquid–vapour surface tension, C ethanol concentration, μ liquid dynamic viscosity, D_l is ethanol diffusivity in water and L a characteristic lengthscale. In order for the flow to ensue, a threshold represented by critical numbers must be surpassed. Ethanol being lighter than water and more volatile will tend to concentrate near the interface. Having the lightest component on top will lead to a stable configuration, as far as Rayleigh-driven convection is concerned. We have also estimated the Bond number, $Bo = (\rho L^2 g)/\gamma$, which was found to be of the order of 0.1. This implies that drops will not be deformed by gravity and will adopt a spherical shape.

The convection revealed by the experiments in the present study is unlikely to be buoyancy driven since the sizes of the drops were very small, i.e. below the capillary length. In addition, the comparison between mixture drops and pure ones ruled out buoyancy-driven flows. If gravity was driving vortices during the first stage of evaporation, this should also be noticeable for the pure drops. The fact that no vortices were observed for pure water and pure ethanol cases indicates that gravity can indeed be ruled out. We therefore concluded that buoyancy cannot be the mechanism behind observed multi-vortices convection. The two remaining mechanisms for convection are surface-tension-driven flows either thermocapillary or solutal in nature. In order to assess any contribution of thermocapillarity to the observed flow, we used infrared thermography as a non-intrusive technique to map the liquid interface temperature. The collected data showed small but measurable variations. We estimated the thermal Marangoni dimensionless number based on recorded temperature differences and we found this to be sub-critical in all cases. Therefore, we concluded that the observed flow convection was more likely to be of solutal Marangoni in nature. An additional flow mechanism is related to continuity, Deegan *et al.* (1997). This flow is due to higher evaporation near the contact line. It is believed to be present for both binary and pure drops and in all stages of evaporation.

Based on the experimental observations, we can propose a scenario for the development of concentration gradients leading to convection vortices. Whilst at $t = 0$ the concentration is uniform, subsequently and because of selective evaporation, ethanol is quickly depleted at the interface as it preferentially evaporates. Furthermore, evaporation is not uniform along the interface, being highest near the contact line. This creates a concentration gradient between the bulk and the interface, which drives a diffusion flux. In the case of volatile binary drops, the amount of ethanol is limited and depends essentially on the initial concentration. Because of the limited 'reservoir' of ethanol, this tends to be depleted as evaporation progresses. As a result, both concentrations in the bulk and on the interface tend to reduce in time. Concentration gradients between the bulk and the interface are good indicators of the gradients along the interface. Indeed, any gradient developing on the interface

https://doi.org/10.1017/jfm.2014.220 Published online by Cambridge University Press

will be at best of the same magnitude as the difference between the bulk and the interface. Figure 11 (appendix A) gives a qualitative understanding of the evolution of various concentrations and gradients for the diffusive case. The presence of convection during the first stage however, is likely to induce mixing and would tend to smooth concentration gradients.

In what follows we attempt a quantitative analysis of the experimental data, including evaporation rates and profile measurements. Starting from the evaporation rate evolution presented in figure 2, we calculate the flow velocity driven by continuity within the drop. This velocity is then used to estimate the Reynolds number, $Re = (\rho V_{continuity} L)/\mu$, which will be representative of the magnitude of the flow driven by continuity. We then use the same evaporation rate data to find the evolution of ethanol concentration within the drop in time. The only assumption made at this stage is that the volume evaporated during the first stage is mainly ethanol, because of preferential evaporation. Based on the evolution of ethanol concentration in time we can then calculate the solutal Marangoni number using the maximum possible concentration difference which can exist along the interface. This is based on the idea that at any given time, the maximum possible (upper limit) concentration difference along the interface corresponds to the situation where at one point the concentration of ethanol is that in the bulk and at another point it would be that of pure water because of evaporation of ethanol. In essence, for all the analysis we use the evaporation rates measured from drop shape analysis to deduce the evolution of concentration gradients. As evaporation is not uniform along the interface, being highest near the contact line, some areas of the interface will be depleted in ethanol whilst other will have the same ethanol content as the bulk. This is the most extreme case where a maximum concentration difference is envisaged. This allows us to estimate the maximum possible concentration gradient along the interface as $\Delta C_{Max} = C_{Max} - 0$.

The flow velocity in the liquid adjacent to the interface, along which the gradient exists, and which is a result of solutal capillary stress is given by $V_{Ma} \sim Ma$. The velocity due to gradients in concentration is proportional to the Marangoni number estimated using concentration gradients along the interface. We can thus compare the ratio between the two velocities within the drop: Marangoni-driven flow and continuity-driven flow, i.e. V_{Ma}/V_{Re} which is equivalent to taking the ratio Ma/Re, expressing the relative magnitudes of the flow driven by the solutal Marangoni effect and by continuity. The ratio is good indicator of which of the two effects is dominant and hence can clearly describe transition from one stage of evaporation to another. The flow structure during stage II is a transition where Marangoni-driven flow is weakening and continuity-driven flow is taking over. The flow velocity during stage I is related to the magnitude of the solutal Marangoni number while that in stage III can be described by a Reynolds number based on the velocity of outward flow. In order to compare these two flows, we can take the ratio of the Marangoni number and Reynolds number, $(Ma_s/Re) \sim (V_{Marangoni}/V_{continuity})$. This ratio yields a new number $(Ma_s/Re) = ((\partial\gamma/\partial C)\Delta C)/(\rho V_{continuity} D_l)$. This new ratio is relevant to all situations where there are solutal-Marangoni-driven flows adjacent to an interface with a drift current in the underlying liquid. Indeed in any configuration where solutal Marangoni flow driven by gradients along the interface is simultaneously taking place with an underlying flow in the bulk of the liquid, the new dimensionless number will be of relevance.

A graph showing the evolution of the ratio Ma_s/Re is presented in figure 7 and in dimensional form in figure 8(*b*). The results presented in figure 7 are calculated

https://doi.org/10.1017/jfm.2014.220 Published online by Cambridge University Press

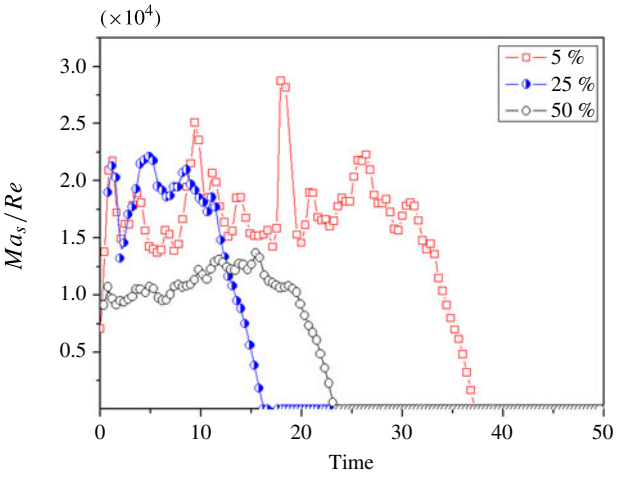


FIGURE 7. (Colour online) Evolution of the ratio (Ma_s/Re) which reflects the three successive stages identified with PIV.

according to the procedure explained above. That is, using the data about evaporation rates and droplet profiles, given in figure 2, the flow velocity due to continuity is deduced since the flow has to compensate exactly for the evaporated mass. We estimated this velocity at a position halfway between the centre of the drop and the contact line, i.e. at $r = R/2$. This velocity due to mass conservation is used to calculate the Reynolds number. Furthermore, the velocity of the flow calculated using evaporation rate data, figure 2, is compared to direct measurements of the flow obtained using PIV as described in Christy *et al.* (2011) and Hamamoto *et al.* (2011). The agreement is very satisfactory: the order of magnitude of velocities calculated from the evaporation rate and using continuity are of the order of 10^{-5} m s^{-1}, which is the same as the experimental PIV measurements. When normalised with the initial values, the ratio Ma_s/Re clearly reflects the evolution of normalised and initialised vorticities evolution in time as shown in figure 8(*a*,*b*).

3.2. *Second stage of evaporation, viscous dissipation and flow transition*

In this section, we analyse the second stage of evaporation and flow structure. This stage is characterised by a transition in flow structure, from multiple vortices to an outward flow. The transition is sudden and a rapid decrease of the magnitude of vorticity is observed.

Since transition in flow occurs at the end of stage I, which corresponds to the depletion of ethanol content, diffusion of this latter in water is examined. This diffusion is obviously a crucial step in sustaining concentration gradients on the interface which might explain flow transition. The diffusion coefficient of ethanol in water is of the order of 1.5×10^{-9} m^{-2} s^{-1}. Assuming a diffusion length scale of the order of the radius of the drop, i.e. 10^{-3} m, one obtains a time of the order of 1000 s. This is three orders of magnitude larger than the transition time, which is of the order of seconds. Hence, diffusion of ethanol alone cannot be a satisfactory explanation for the observed transition in flow. An alternative physical mechanism to be considered is viscous dissipation. Indeed, once the driving force for solutal

https://doi.org/10.1017/jfm.2014.220 Published online by Cambridge University Press

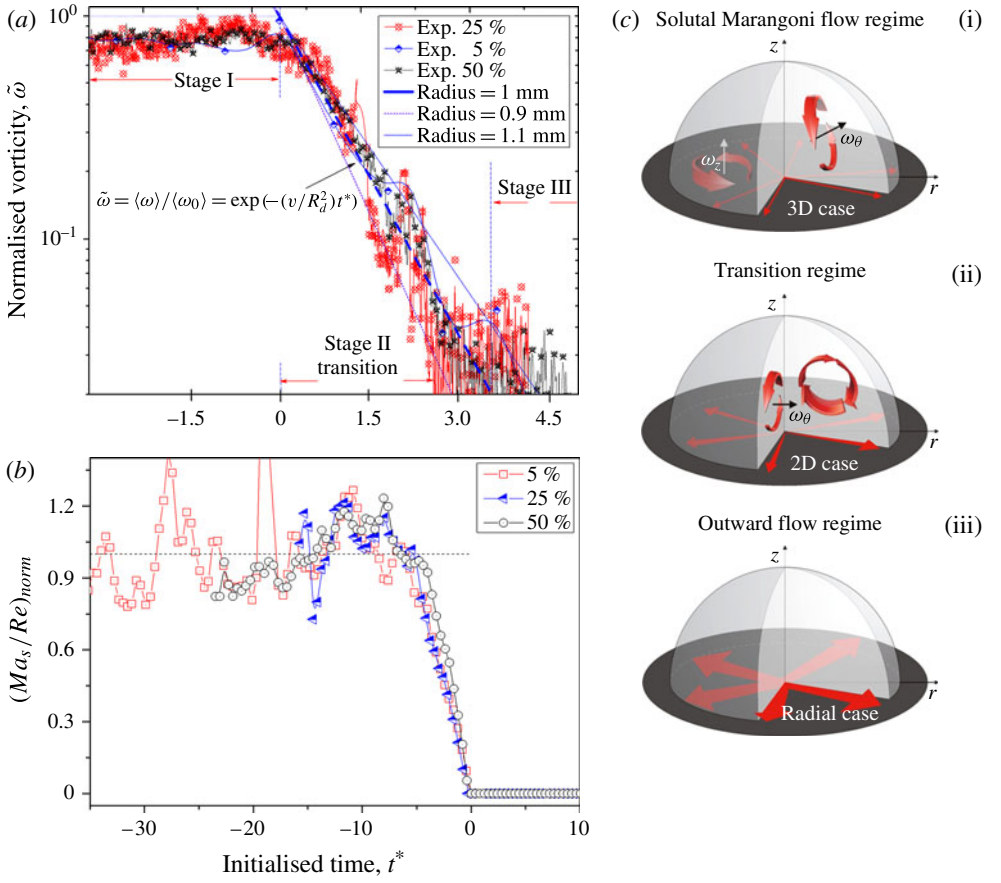


FIGURE 8. (Colour online) Stages of the flow: (*a*) normalised experimental vorticity, (*b*) ratio of solutal Marangoni number and Reynolds number evolution and (*c*) illustration of the flow stages.

Marangoni flow switches off, the flow decays under the resistance of viscosity. This mechanism will be examined below.

The evolution of the flow (represented by average vorticity) with the initial condition, at $t = 0$, $\omega = \omega_0$ and subsequently dampened by viscous dissipation is examined. The evolution within the droplet is governed by the incompressible Navier–Stokes conservation equation when expressed in terms of vorticity, $\omega = \nabla \times \boldsymbol{V}$, is given by

$$\frac{\partial \omega}{\partial t} + \boldsymbol{V} \cdot \nabla \omega = \boldsymbol{\omega} \cdot \nabla V + \nu \nabla^2 \omega. \tag{3.1}$$

The approximate solution for viscous dissipation is given by (see appendix B for further details)

$$\langle\omega\rangle \sim \langle\omega_0\rangle \exp\left(-\nu t^*/R_d^2\right), \tag{3.2}$$

where $\langle\omega\rangle$ is the space-averaged vorticity. For the considered experimental cases, drop radii are of the order of $R_d \approx 10^{-3}$ m and the kinematic viscosity is taken as that of water, hence of the order $\nu \approx 10^{-6}$ m^2 s^{-1}. The value of viscosity is assumed as that of water since transition occurs at the end of the first stage, so most of ethanol would

https://doi.org/10.1017/jfm.2014.220 Published online by Cambridge University Press

have completely evaporated. Using these values for radius and viscosity, one obtains, for a millimetre drop base radius, $\nu/R_d^2 \approx 1$. This is the case for 25 % concentration. From (3.2), it can be noted that the exponential decay constant changes slightly with drop base radius, so for our experiments ν/R_d^2 ranges from 0.83 to 1.23 for 5 % to 50 % initial ethanol concentration. However, it is expected that for same sized drops, the evolution of vorticity during the transition stage to be the same. It is noteworthy that the hypothesis of viscous damping of the flow leads to an order of magnitude for the duration of transition comparable to the one revealed by experiments, see figure 6. Furthermore, when normalised with the initial value, the transition in flow is found to be the same regardless of the initial concentration, figure 8(*a*).

3.3. *Last stage of evaporation, outward flow*

The last stage of evaporation is characterised by an outward flow which accelerates in time. The outward flow is the result of continuity driven by evaporation at the contact line. This flow due to mass conservation was first reported by Deegan *et al.* (1997). It was found responsible for the 'coffee ring' stain formation observed whenever suspension drops evaporate. The outward flow during the last stage of evaporation exhibits an increasing flow velocity (Marin *et al.* 2011). The flow velocity can be an order of magnitude greater than at the start of the evaporation. This is due to thinning of the drop and the reduction of area available for flow which has to compensate for evaporation (Hamamoto *et al.* 2011), see figure 9. In figure 10 the spatio-temporal flow field during the evaporation of a pure water drop is compared with that of a 5 % ethanol drop during its last stage of evaporation. The comparison clearly shows that the two spatio-temporal profiles are similar qualitatively and quantitatively: the order of magnitude of radial velocities, the radial profile and time evolution are comparable. Note also that these orders of magnitude of flow velocities are comparable to the ones calculated using evaporation rates from figure 2, as discussed previously.

4. Discussion and conclusions

The study of evaporation and the internal flow field in binary drops revealed three distinct stages of evaporation and flow structure. Because of selective evaporation, ethanol (the more volatile component) diffuses from the bulk to the interface where it evaporates. The non-uniform evaporation and the fact it is localised near the three-phase contact line is well established (Deegan *et al.* 1997). This non-uniformity in evaporation induces concentration gradients along the interface. Such gradients induce surface tension gradients, which are the driving force for flow motion expressed as $(\partial u_\theta/\partial n) \backsimeq -Ma_s(\partial C_i/\partial \tau)$, here the solutal Marangoni number is given by, $Ma_s \backsimeq -(\partial \gamma/\partial n)\Delta C(R_d/(\mu D_l))$. The non-uniform distribution of evaporation along the interface leads to local concentration gradients, which generate surface tension gradients and lead to solutal Marangoni flow. By the end of the first stage, most (if not all) ethanol would have evaporated. Concentration gradients are therefore too weak to sustain the flow, i.e. the solutal Marangoni number becomes sub-critical. Once the driving force for the flow switches off, the flow evolution is dictated by viscous forces. The decay in vorticity intensity is entirely controlled by viscous dissipation. This transition stage exhibits an exponential evolution in time, starting from the initial vorticity and finishing when this vanishes. The last stage is reminiscent of the pure water case where an outward flow is observed. The monotonic outward flow during the last stage is shown to result from continuity (Hamamoto *et al.* 2011). This is due to the fact that evaporation takes place exclusively near the three-phase

https://doi.org/10.1017/jfm.2014.220 Published online by Cambridge University Press

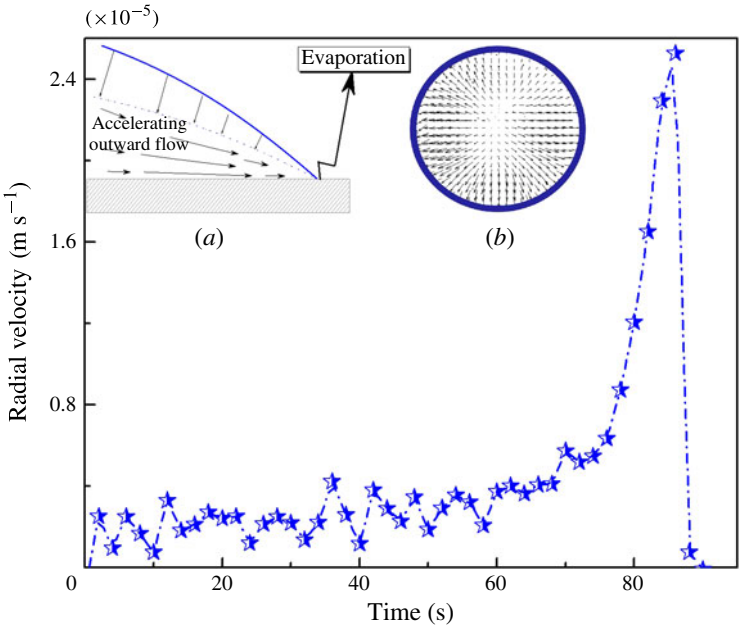


FIGURE 9. (Colour online) Measured radial velocity over time $0.1R$ from contact line. Inset: (*a*) sketch of outward flow driven by continuity, (*b*) PIV data for outward flow. This is observed during the last stage of evaporation of binary drops and pure water ones, see Hamamoto *et al.* (2011) and Marin *et al.* (2011).

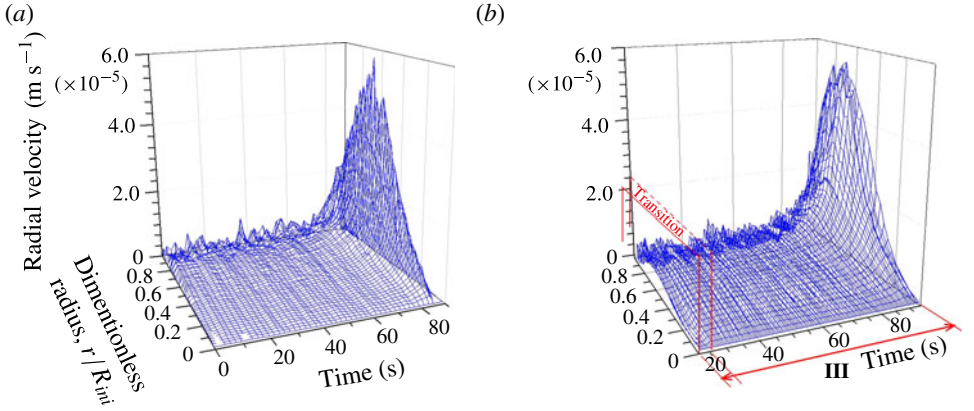


FIGURE 10. (Colour online) Spatio-temporal flow profile for (*a*) pure water drop, (*b*) the last stage of evaporation of a 5 % ethanol drop.

contact line, consequently the flow in the drop is driven to compensate for mass loss by evaporation. The observation that regardless of the initial concentration, the transition in flow is virtually the same is strong support of this analysis. Indeed, the experimental data span a wide range of concentrations. Despite this, the transition in flow is found to occur in the same fashion.

The transition between the first stage where the flow structure is dominated by vigorous multiple vortices to an outward flow, indicates that stage I is dominated

https://doi.org/10.1017/jfm.2014.220 Published online by Cambridge University Press

by Marangoni flow driven by concentration gradients on the interface. The flow during this stage is inherently three-dimensional and asymmetrical, whereas the flow structure in stage III is more one-dimensional and symmetrical, figure 8(*c*). During the first stage of evaporation, concentration gradients at the interface are large enough to induce the vigorous observed flow structure. In comparison the flow driven by mass conservation (continuity) is negligible during this first phase of evaporation. As evaporation proceeds, concentration gradients and hence the solutal Marangoni number weaken and then continuity-driven flow starts to take over. Following the flow transition and during stage III, the outward flow driven by mass conservation (continuity) becomes dominant and the solutal Marangoni flow is negligible. This evolution of flow structure and the distinct stages are found to be well described by the ratio of the two dimensionless numbers, Ma_s/Re.

A simple analysis yielded expression (3.2) which describes the evolution of vorticity in time, initially at ω_0 and then decaying under the resistance of viscosity. This expression in its normalised form is independent of initial concentration; the dimensional vorticity however does depend on the initial concentration through the initial vorticity ω_0. The relation between the initial vorticity and initial concentration is beyond the scope of the present analysis which aims primarily to address the question of the mechanism behind the transition in flow. The average vorticities from figure 6 are normalised by the initial vorticity (from the first stage) and time is initialised by transition time. The normalised vorticities are then plotted for the three initial concentrations on the same graph in figure 8(*a*), which shows that data for different initial concentrations collapse onto a single curve (for similar sized drops) which reveals the three distinct stages in flow structure. The expression for dimensionless vorticity obtained in (3.2) is then superimposed on the experimental data for all concentrations. The agreement is more than satisfactory in view of the simple analytical exponential decay in vorticity. The slope of the transition decay is affected by the drop size, figure 8(*a*). Considering that no fitting parameters or adjustment factors are used in the comparison, the achieved agreement is strong support for the hypothesis of a viscous dissipation mechanism which controls transition of the flow.

Finally, the observation that during the first stage of evaporation, the number of vortices reduces as evaporation progresses is an interesting trend. The fact that concentration gradients, which are the driving force for the flow, are also decreasing during the first stage, raises the question of the correlation between the two, i.e. the number of vortices and concentration gradients. We can only speculate at this point about the analogy between these observations and turbulence versus energy dissipation. This remains however an open question revealed by this study, worth the attention of researchers in the field. Nonetheless, and despite outstanding questions, the presented study is pioneering in the investigation of internal flow in volatile mixture drops. The implications of the internal flow and its behaviour is crucial in understanding energy transport mechanisms in these systems. The obtained results illustrate that, besides the complex transient and multiple cells observed, solutal gradients are the origin of the flow and reveal the existence of a threshold below which the flow driving force becomes too weak to sustain flow.

Acknowledgements

The authors would like to acknowledge the contribution of Y. Hamamoto and J. Christy to the experimental part of this study as well as O. Rahli for assistance in producing illustration in figure 8(*c*). The authors are indebted to Professor A. Steinchen-Sanfeld for constructive discussions on this project.

https://doi.org/10.1017/jfm.2014.220 Published online by Cambridge University Press

Appendix A

In addition to the above analysis, diffusion can be solved within the drop to deduce concentrations and their evolution with time. In the case of the evaporation of binary drops the more volatile component evaporates first because of selective evaporation. This component diffuses from the bulk of the drop to the interface to evaporate. The evaporated component then diffuses in the gas phase which is a mixture of air and vapour. The diffusion equation in a liquid domain can be written as follows:

$$\frac{\partial C}{\partial t} = D_l \nabla^2 C \tag{A 1}$$

where D_l is the diffusion coefficient of ethanol in water (in liquid phase).

The boundary conditions are: at $t = 0$, $C(r, \theta, 0) = C_0$ and at the substrate interface, $z = 0$, $\partial C/\partial z|_{z=0} = 0$.

At $t > 0$ and on interface $R = s(\theta)$,

$$\left.\frac{\partial C}{\partial n}\right|_{int} = h\,(C_{int} - C_\infty)\,, \tag{A 2}$$

where h is the diffusion–convection coefficient on the liquid–air interface including the modifying coefficient from gas to liquid ethanol concentration. Using the characteristic length $L_{ref} = R_d$, $\Delta C = C_0 - C_\infty$ (C_∞ is equal to zero in the present study as no ethanol is contained in the air) and $\tau_{ref} = R_d^2/D_l$ the equation becomes

$$\frac{\partial C^*}{\partial Fi} = \nabla^{*2} C \tag{A 3}$$

and

$$\left.\frac{\partial C^*}{\partial n^*}\right|_{int} = Bi_s C^*_{int}. \tag{A 4}$$

The solutal Biot and Fick numbers are $Bi_s = hR_d/D_l$, $Fi = D_l t/R_d^2$, respectively.

This linear problem has an analytical solution using separation of variables (or Laplace transformation and Green function)

$$C^*(r, t) = \frac{(C(r, t) - C_\infty)}{(C_0 - C_\infty)} = \frac{2}{r/R_d}\sum_{n=1}^{\infty} \mathrm{e}^{-Fi}\frac{\sin(\lambda_n) - \lambda_n \cos(\lambda_n)}{\lambda_n^2\,[\lambda_n - \sin(\lambda_n)\cos(\lambda_n)]}\sin\left(\lambda_n \frac{r}{R_d}\right), \tag{A 5}$$

where the eigenvalues λ_n are the solutions of the equation $\lambda \cot(\lambda) = (1 - Bi_s)$.

The surface concentration is obtained (see figure 11) for $r = R_d$ and that in the centre (bulk) is deduced for $r \to 0$ and given by

$$C^*(0, t) = \frac{C(0, t) - C_\infty}{(C_0 - C_\infty)} = 2\sum_{n=1}^{\infty} \mathrm{e}^{-Fi}\frac{\sin(\lambda_n) - \lambda_n \cos(\lambda_n)}{\lambda_n - \sin(\lambda_n)\cos(\lambda_n)}. \tag{A 6}$$

Appendix B

In what follows, we propose a scale analysis description of the flow time evolution (represented by average vorticity) with the initial condition, at $t = 0$, $\omega = \omega_0$ and subsequently damped by viscous dissipation. The flow of a vortex within the droplet is

https://doi.org/10.1017/jfm.2014.220 Published online by Cambridge University Press

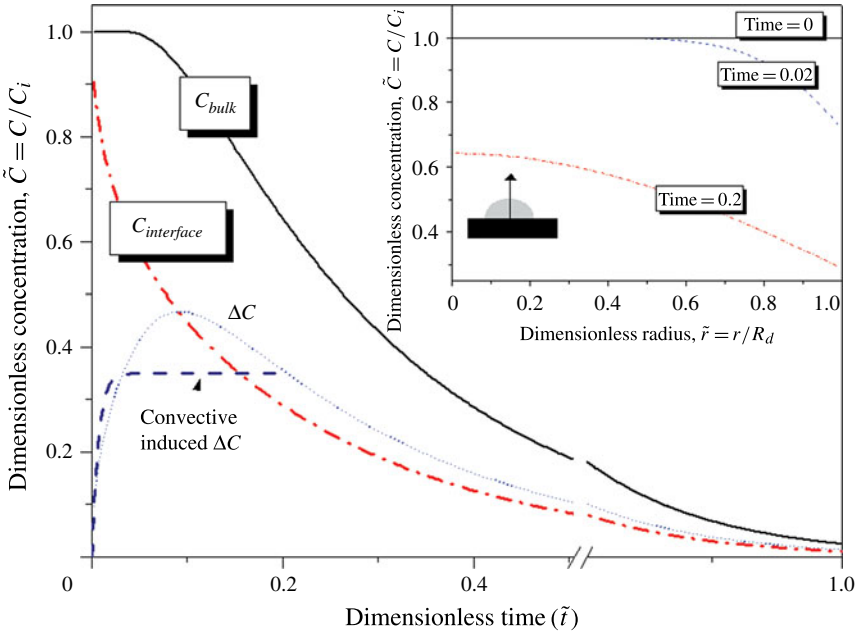


FIGURE 11. (Colour online) Dimensionless concentrations and gradient evolution in a diffusive mode, versus both time and radius.

governed by the incompressible Navier–Stokes conservation equation when expressed in terms of vorticity, $\omega = \nabla \times \boldsymbol{V}$, given by

$$\frac{\partial \omega}{\partial t} = \nu \nabla^2 \omega + \overbrace{\boldsymbol{\omega} \cdot \nabla \boldsymbol{V} - \boldsymbol{V} \cdot \nabla \omega}^{inducing\ \ vortex\ \ deformation} + \overbrace{S}^{barocline\ \ production}. \tag{B 1}$$

In order to capture the scale order, we use the assumption of weak vortex deformation or equivalent order, i.e. $\boldsymbol{V} \cdot \nabla \omega \approx \boldsymbol{\omega} \cdot \nabla \boldsymbol{V}$ (or two-dimensional main flow, with axial symmetry) and negligible source term S ($\nabla p \cdot \nabla \rho \approx 0$ and $\nabla \sigma \approx 0$) so we obtain,

$$\frac{\partial \omega}{\partial t} \approx \nu \nabla^2 \omega. \tag{B 2}$$

Based on previous space and time reference scales (appendix A) we get

$$\frac{\partial \omega}{\partial F_\nu} \approx \nabla^2 \omega \tag{B 3}$$

where $F_\nu = \nu t^*/R_d^2$. Expressed on the given volume area Ω,

$$\int_\Omega \frac{\partial \omega}{\partial F_\nu} \mathrm{d}\Omega \approx \int_\Omega \nabla^2 \omega \mathrm{d}\Omega \tag{B 4}$$

based on classical Reynolds transport theorem (neglecting $V\boldsymbol{n} \cdot \omega$) and Green–Ostrogradski theorem it becomes,

$$\Omega \frac{\partial \langle \omega \rangle}{\partial F_\nu} \approx \int_\Sigma \nabla \omega \cdot \boldsymbol{n} \ \mathrm{d}\Sigma \tag{B 5}$$

https://doi.org/10.1017/jfm.2014.220 Published online by Cambridge University Press

where $\langle\omega\rangle$ is the space-averaged vorticity. The surface-normal vector $\boldsymbol{n}$ and interface are related to the droplet radius. Due to the free surface condition, the main vorticity gradient is on the droplet base (substrate/liquid interface) $\int_{\Sigma} \nabla\omega \cdot \boldsymbol{n} \mathrm{d}\Sigma \approx \int_{\bar{r}=0}^{1} \nabla\omega|_{z=0}\ 2\pi\bar{r}\mathrm{d}\bar{r}$. We will keep only the main order of the damping effect using the non-slip boundary condition on the substrate $\nabla\omega|_{z=0} \sim (-\omega/1)$. The dimensionless spatial variable $\bar{r} \in [\![0; 1]\!]$.

Based on the vorticity damping tendency we can obtain

$$\frac{\partial\langle\omega\rangle}{\partial F_v} \sim -\langle\omega\rangle, \quad \int_{\langle\omega_0\rangle}^{\langle\omega\rangle} \frac{\partial\langle\omega\rangle}{\langle\omega\rangle} \sim \int_0^{F_v} -\partial F_v \tag{B 6a,b}$$

The solution is an exponential decaying one, illustrating the vorticity damping due to viscous effects, $\langle\omega\rangle/\langle\omega_0\rangle \sim \mathrm{e}^{-F_v}$, or

$$\langle\omega\rangle \sim \langle\omega_0\rangle \exp -\nu t^*/R_d^2. \tag{B 7}$$

REFERENCES

CHENG, A. K. H., SOOLAMAN, D. M. & YU, H. 2006 Evaporation of micro droplets of ethanol–water mixtures on gold surfaces modified with self-assembled monolayers. *J. Phys. Chem.* B **110**, 11267–11271.

CHRISTY, J., HAMAMOTO, Y. & SEFIANE, K. 2011 Flow transition within an evaporating binary mixture sessile drop. *Phys. Rev. Lett.* **106**, 205701.

DEEGAN, R. D., BAKAJIN, O., DUPONT, T. F., HUBER, G., NAGEL, S. R. & WITTEN, T. A. 1997 Capillary flow as the cause of ring stains from dried liquid drops. *Nature* **389**, 827–829.

ERBIL, H. Y. 2012 Evaporation of pure liquid sessile and spherical suspended drops: a review. *Adv. Colloid Interface Sci.* **170**, 67–86.

GHASEMI, H. & WARD, C. A. 2010 Energy transport by thermocapillary convection during sessile-water-droplet evaporation. *Phys. Rev. Lett.* **13**, 136102.

HAMAMOTO, Y., CHRISTY, J. R. E. & SEFIANE, K. 2011 Order-of-magnitude increase in flow velocity driven by mass conservation during the evaporation of sessile drops. *Phys. Rev.* E **83**, 051602.

HOPKINS, R. J. & REID, J. P. 2006 A comparative study of the mass and heat transfer dynamics of evaporating ethanol/water, methanol/water, and 1-propanol/water aerosol droplets. *J. Phys. Chem.* B **110**, 3239–3249.

HU, H. & LARSON, R. G. 2006 Marangoni effect reverses coffee-ring depositions. *J. Phys. Chem.* B **110**, 7090–7094.

MARIN, A. G., GELDERBLOM, H., LOHSE, D. & SNOEIJER, J. H. 2011 Rush-hour in evaporating coffee drops. *Phys. Fluids* **23**, 091111.

RISTENPART, W. D., KIM, P. G., DOMINGUES, C., WAN, J. & STONE, H. A. 2007 Influence of substrate conductivity on circulation reversal in evaporating drops. *Phys. Rev. Lett.* **99**, 234502.

ROWAN, S. M., NEWTON, M. I., DRIEWER, F. W. & MCHALE, G. J. 2000 Evaporation of microdroplets of azeotropic liquids. *J. Phys. Chem.* B **104**, 8217–8220.

SEFIANE, K. & BENNACER, R. 2011 An expression for droplet evaporation incorporating thermal effects. *J. Fluid Mech.* **667**, 260–271.

SEFIANE, K., DAVID, S. & SHANAHAN, M. E. R. 2008 Wetting and evaporation of binary mixture drops. *J. Phys. Chem.* B **112**, 11317–11323.

SEFIANE, K., WILSON, S. K., DAVID, S., DUNN, G. & DUFFY, B. R. 2009 On the effect of the atmosphere on the evaporation of sessile droplets of water. *Phys. Fluids* **21**, 062101.

YOUNG, T. 1805 An essay on the cohesion of fluids. *Phil. Trans. R. Soc. Lond.* **95**, 65–87.

https://doi.org/10.1017/jfm.2014.220 Published online by Cambridge University Press